International Journal Of Advancement In Engineering Technology, Management and Applied Science (IJAETMAS)

ISSN: 2349-3224 || www.ijaetmas.com || Volume 04 - Issue 09 || September-2017 || PP. 33-42

Numerical Simulation for GMAW with an Energy Law Preserving Method

Yongyue Jiang[1,3], Lin Li[2,*]

[1]*Beijing Time Technologies Co., Ltd., Kaituo Road 17, Beijing 100085, China.*

[2]*School of Mathematics and Physics, University of South China, Hengyang 421000, China.*

[3]*School of Civil & Environmental Engineering, University of Science and Technology Beijing, Beijing 100083, China.*

***Abstract*- In this paper, we take a numerical investigation for GMAW with an energy law preserving method and a new model including Navier-Stokes equation, the phase field model, energy equation and Maxwell's equation. We derived the continuous and discrete energy law for GMAW never published before. We treat the mass conservation equation with the penalty formulation and discretize the model with a modified midpoint scheme. The spray transfer especially the projected transfer in GMAW is computed as the numerical example with constant current set as welding current to investigate the evolution of interface change in metal transfer. From these numerical solutions and results compared with the result of reference paper and high-speed photography, the accuracy of the model and the method are validated easily and the result with the relative coarse grid is the same as the result with finer grid.**

Keywords*- *GMAW; Phase field model; Energy law preserving method; Spray transfer; Finite element method

I. INTRODUCTION

Gas metal arc welding (GMAW) uses the arc between two electrodes to melt the work-piece for joining. Be different of other arc welding method, GMAW chooses the wire as the electrode and the wire would be molten with the heat of arc, Ohmic heating and heat produced by electrodes. It is widely used in industry due to the high efficiency, excellent quality and low cost and so on. In free flight transfer mode, the liquid melt becomes a suspending droplet with the influence of surface tension from the electrode and liquid melt itself. As the welding wire keeps melting and other forces like electromagnetic forces acts on the droplet, the droplet will break up and fall into the arc zone and then weld pool. This whole process is called metal transfer which plays an important role in GMAW. The purpose of the theoretical research for metal transfer is that they want to make good prediction for the geometry and the size of the droplet with a high precision and also the weld pool. Mckelliget and Szekely [1] proposed a steady mathematical model to investigate velocity and temperature of electrode and weld pool in early time but not the dynamic process of metal transfer. Haidar and Lowke [2] investigated the influence of different currents on the size of droplets. Cheng, Wu and Lian [3] presented a dynamic model for metal transfer combined with electromagnetic theory and volume of fluid (VOF) considering electromagnetic force, surface tension and arc plasma. A unified comprehensive model was developed by Hu and Tsai [4] to simulate the transport phenomena occurring during the gas metal arc welding like melting of the electrode, droplet formation, detachment and weld pool dynamics. But still, they used VOF to simulate the interface of multi-phase fluids. Murphy [5] presented a self-consistent three-dimensional model of GMAW for simulating

ISSN: 2349-3224 || www.ijaetmas.com || Volume 04 - Issue 09 || September-2017 || PP. 33-42

the arc, electrode and welding pool which still a steady model without the consideration of metal transfer. Haidar [6] developed a two-dimensional dynamic theory for predictions of arc and electrode properties in arc welding and used this model to investigate the heat and mass transfer in GMAW.

In VOF method, thermocapillary effect and mixture energy are not in consideration which play important roles in the theoretical research of multi-phase fluids flow, heat and mass transfer with clear interface. Thermocapillary effect is widely studied in Marangoni convection [7] exists in the multi-phase fluids system where the surface tension becomes dominant [8]-[10]. Phase field model may be more suitable than VOF as this method introduces the thickness of interface into the model which should exists in VOF and it considers the mixture energy in the phase field model (e.g. [11], [12]). It does not regard the interface as a boundary and it avoids dealing with the jump of boundary conditions in the phase field model.

There are lots of available numerical methods used to solve the phase field model including spectral method [13], adaptive moving mesh method [14], finite element method [15] and finite difference method [16]. The energy stable scheme can make the numerical result closer to reality which can derived a physical energy law usually exists in the phase field model. Two efficient and unconditionally energy stable numerical schemes for NSCH with static contact line condition were developed by H. Yu and X. Yang and they got a discrete energy law inequality [17]. The preservation of energy law has been turned out to be important in designing a numerical method as this method preserving energy law can produce the correct solution even though a rapid change or singularity occurs in the computation (e.g. [15], [18], [19]).

In this paper, we develop an energy law preserving method for GMAW and derive a continuous energy law. The model of the system, boundary conditions as well as its weak formulation and continuous energy law are introduced in Section 2. In Section 3, we present the fully discretized NSCH system and the discrete energy law. The result of metal transfer with constant current and the comparison among our numerical solution, reference paper and high-speed photography are discussed in Section 4. Section 5 is conclusion.

II. SYSTEM of GMAW, WEAK FORM and ENERGY LAW

Fig. 1 shows the general physical model of GMAW which is also the computing domain. The welding region is defined as Ω a bounded domain and Γ is the boundary of Ω.

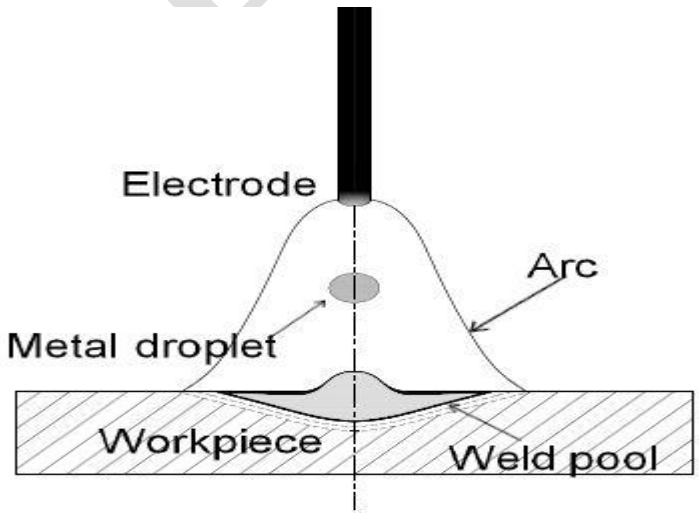

Fig. 1 The simple structure of GMAW system.

ISSN: 2349-3224 || www.ijaetmas.com || Volume 04 - Issue 09 || September-2017 || PP. 33-42

The theoretical model with phase field model for GMAW is shown as follows (Eq. (3) and (4) are the phase field model of Cahn-Hilliard type):

$$\frac{\partial \rho}{\partial t}+\nabla\cdot(\rho\mathbf{v})=0 \tag{1}$$

$$\frac{\partial(\rho\mathbf{v})}{\partial t}+\nabla\cdot(\rho\mathbf{v}\otimes\mathbf{v})=-\nabla p+\nabla\cdot\left(\eta\left(\nabla\mathbf{v}+\nabla\mathbf{v}^{\mathrm{T}}\right)\right)+\mu\nabla f+\rho\mathbf{G}+\mathbf{J}\times\mathbf{B} \tag{2}$$

$$\frac{\partial f}{\partial t}+\mathbf{v}\cdot\nabla f=\nabla\cdot(M\nabla\mu) \tag{3}$$

$$\mu=\frac{f\left(f^2-1\right)}{\varepsilon}-\varepsilon\Delta f \tag{4}$$

$$\frac{\partial(\rho c_p T)}{\partial t}+\nabla\cdot(\rho c_p\mathbf{v}T)=\nabla\cdot(k\nabla T)-\rho H\frac{\partial f}{\partial t}+\frac{\mathbf{J}^2}{\sigma_e}+\frac{5k_b}{2e}\mathbf{J}\cdot\nabla T \tag{5}$$

$$\Delta\mathbf{A}=-\mu_0\mathbf{J},\ \mathbf{J}=-\sigma_e\nabla\Phi,\ \nabla\cdot(\sigma_e\nabla\Phi)=0,\ \mathbf{B}=\nabla\times\mathbf{A} \tag{6}$$

Here $M,\varepsilon,\rho,\eta,k,c_p,e,\sigma_e$ are the phenological mobility coefficient, thickness of interface, density, viscosity, thermal conductivity coefficient, specific heat, electronic charge and electrical conductivity, respectively. μ in Eq. (4) is called chemical potential which represents the mixture energy as it has two parts contributing to separation and mixing, respectively. f is an order parameter for defining different phases of the mixture ($f=1$: fluid and $f=-1$: metal). $\mathbf{G}=(0,-9.8)$ represents the gravitational acceleration. The third term on the right-hand side of Eq. (2) represents the capillary force due to the mixture energy and different properties of different phases. $\Phi,\mathbf{B},\mathbf{A}$ are the electrical potential, self-induced electro-magnetic field and magnetic vector. The boundary conditions and computing domain in the previous work of Hu and Tsai [4] are used in this paper. The additional boundary conditions are $\partial_{\mathbf{n}}f=0,\partial_{\mathbf{n}}\mu=0$. As the densities of molten metal and solid metal are matched, the model of the system can be simplified in the next form

$$\nabla\cdot\mathbf{v}=0 \tag{7}$$

$$\rho\frac{\partial\mathbf{v}}{\partial t}+\rho(\mathbf{v}\cdot\nabla)\mathbf{v}=-\nabla p+\eta\Delta\mathbf{v}+\mu\nabla f+\rho\mathbf{G}+\mathbf{J}\times\mathbf{B} \tag{8}$$

$$\frac{\partial f}{\partial t}+\mathbf{v}\cdot\nabla f=M\Delta\mu \tag{9}$$

$$\mu=\frac{f\left(f^2-1\right)}{\varepsilon}-\varepsilon\Delta f \tag{10}$$

$$\rho c_p\frac{\partial T}{\partial t}+\rho c_p\mathbf{v}\cdot\nabla T=\nabla\cdot(k\nabla T)-\rho H\frac{\partial f}{\partial t}+\frac{\mathbf{J}^2}{\sigma_e}+\frac{5k_b}{2e}\mathbf{J}\cdot\nabla T \tag{11}$$

$$\Delta\mathbf{A}=-\mu_0\mathbf{J},\ \mathbf{J}=-\sigma_e\nabla\Phi,\ \nabla\cdot(\sigma_e\nabla\Phi)=0,\ \mathbf{B}=\nabla\times\mathbf{A} \tag{12}$$

A positive constant c (e.g. [15], [19]) is introduced to rewrite Eq. (9) and (10) for the stability as $\mu=\omega+cf$ $\frac{\partial f}{\partial t}+\mathbf{v}\cdot\nabla f=M\Delta(\omega+cf)$.

Denote $\mathbf{W}^{1,3}(\Omega)=\left(W^{1,3}(\Omega)\right)^3$, $\mathbf{L}^2(\Omega)=\left(L^2(\Omega)\right)^2$ and $L_0^2(\Omega)=\left\{p\in L^2(\Omega),\int_\Omega p\,d\mathbf{x}=0\right\}$. The weak

ISSN: 2349-3224 || www.ijaetmas.com || Volume 04 - Issue 09 || September-2017 || PP. 33-42

form of the penalized GMAW system reads: Find $\mathbf{v}, \mathbf{J}, \mathbf{B}, \mathbf{A} \in \mathbf{W}^{1,3}(\Omega)$, $p \in L_0^2(\Omega)$, $f, \mu, \Phi, T \in W^{1,3}(\Omega)$ such that

$$\int_\Omega \nabla \cdot \mathbf{v} q d\mathbf{X} = 0$$

$$\forall q \in L_0^2(\Omega) \quad (13)$$

$$\int_\Omega \left(\rho \frac{\partial \mathbf{v}}{\partial t} \cdot \mathbf{u} + \rho (\mathbf{v} \cdot \nabla) \mathbf{v} \cdot \mathbf{u} - p(\nabla \cdot \mathbf{u}) + \eta \nabla \mathbf{v} : \nabla \mathbf{u} - \rho \mathbf{G} \cdot \mathbf{u} - (\mathbf{J} \times \mathbf{B}) \cdot \mathbf{u} - (\omega + cf) \nabla f \cdot \mathbf{u} \right) d\mathbf{x} = 0$$

$$\forall \mathbf{u} \in \mathbf{W}^{1,3} \quad (14)$$

$$\int_\Omega \left(\frac{\partial f}{\partial t} \gamma + (\mathbf{v} \cdot \nabla f) \gamma + M \nabla (\omega + cf) \cdot \nabla \gamma \right) d\mathbf{x} = 0$$

$$\forall \gamma \in W^{1,3} \quad (15)$$

$$\int_\Omega \left((\omega + cf) \chi - \frac{f(f+1)(f-1)}{\varepsilon} \chi - \varepsilon \nabla f \cdot \nabla \chi \right) d\mathbf{x} = 0$$

$$\forall \chi \in W^{1,3} \quad (16)$$

$$\int_\Omega \left(\rho c_p \left(\frac{\partial T}{\partial t} + \mathbf{v} \cdot \nabla T \right) \theta + k \nabla T \cdot \nabla \theta + \rho H \frac{\partial f}{\partial t} \theta - \frac{\mathbf{J}^2}{\sigma_e} \theta - \frac{5 k_b}{2e} \mathbf{J} \cdot \nabla T \theta \right) d\mathbf{x} = 0$$

$$\forall \theta \in W^{1,3} \quad (17)$$

$$\int_\Omega (\nabla \mathbf{A} : \nabla \boldsymbol{\alpha} + \mu_0 \sigma_e \nabla \Phi \cdot \boldsymbol{\alpha}) d\mathbf{x} - \int_\Gamma (\mathbf{n} \cdot \nabla \mathbf{A}) \cdot \boldsymbol{\alpha} ds = 0, \quad \int_\Omega (\sigma_e \nabla \Phi \cdot \nabla \varphi) d\mathbf{x} - \int_\Gamma \sigma_e (\mathbf{n} \cdot \nabla \Phi) \varphi ds = 0,$$

$$\int_\Omega (\mathbf{J} + \sigma_e \nabla \Phi) \cdot \mathbf{S} \, d\mathbf{x} = 0, \quad \int_\Omega (\mathbf{B} - \nabla \times \mathbf{A}) \cdot \mathbf{L} \, d\mathbf{x} = 0$$

$$\forall \boldsymbol{\alpha}, \varphi, \mathbf{S}, \mathbf{L} \in \mathbf{W}^{1,3} \quad (18)$$

Here, we take $\gamma = \omega + cf$, $\mathbf{v} = \mathbf{u}$, $q = p$, $\chi = \partial f / \partial t$, $\theta = T$, $\varphi = \Phi$, $\boldsymbol{\alpha} = \mathbf{A}$, $\mathbf{S} = \mathbf{J}T/\sigma_e$ and $\mathbf{L} = \mu_0 \sigma_e \mathbf{J}$ into Eq. (13)-(18) and the continuous weak form becomes

$$\int_\Omega \nabla \cdot \mathbf{v} p d\mathbf{X} = 0$$

(19)

$$\int_\Omega \left(\rho \frac{\partial}{\partial t} \left(\frac{\mathbf{v}^2}{2} \right) - p(\nabla \cdot \mathbf{v}) + \eta \nabla \mathbf{v} : \nabla \mathbf{v} - \rho \mathbf{G} \cdot \mathbf{v} - (\mathbf{J} \times \mathbf{B}) \cdot \mathbf{v} - (\omega + cf) \nabla f \cdot \mathbf{v} \right) d\mathbf{x} = 0$$

(20)

$$\int_\Omega \left(\frac{\partial f}{\partial t} (\omega + cf) + (\mathbf{v} \cdot \nabla f)(\omega + cf) + M \nabla (\omega + cf) \cdot \nabla (\omega + cf) \right) d\mathbf{x} = 0$$

(21)

ISSN: 2349-3224 || www.ijaetmas.com || Volume 04 - Issue 09 || September-2017 || PP. 33-42

$$\int_\Omega \left((\omega + cf)\frac{\partial f}{\partial t} - \frac{f(f+1)(f-1)}{\varepsilon}\frac{\partial f}{\partial t} - \varepsilon \nabla f \cdot \nabla \frac{\partial f}{\partial t} \right) d\mathbf{x} = 0 \tag{22}$$

$$\int_\Omega \left(\rho c_p \frac{\partial}{\partial t}\left(\frac{T^2}{2}\right) + k\nabla T \cdot \nabla T + \rho H \frac{\partial f}{\partial t} T - \frac{\mathbf{J}^2}{\sigma_e} T - \frac{5k_b}{2e}\mathbf{J} \cdot \nabla \left(\frac{T^2}{2}\right) \right) d\mathbf{x} = 0 \tag{23}$$

$$\int_\Omega \left(\nabla \mathbf{A} : \nabla \mathbf{A} + \mu_0 \sigma_e \nabla \Phi \cdot \mathbf{A}\right) d\mathbf{x} = 0, \ \int_\Omega \left(\sigma_e \nabla \Phi \cdot \nabla \Phi\right) d\mathbf{x} = 0, \tag{24}$$

$$\int_\Omega \left(\mathbf{J} + \sigma_e \nabla \Phi\right) \cdot \frac{\mathbf{J}}{\sigma_e} T \, d\mathbf{x} = 0, \ \int_\Omega \left(\mathbf{B} - \nabla \times \mathbf{A}\right) \cdot \mu_0 \sigma_e \mathbf{J} \, d\mathbf{x} = 0 \tag{25}$$

And then we get the continuous energy law according to Eq. (19) + (20) + (21) — (22) + (23) + (24) — (25):

$$\frac{dE}{dt} = \int_\Omega \left(\rho \mathbf{G} \cdot \mathbf{v} + \left(\mathbf{J} \times \mathbf{B}\right) \cdot \mathbf{v} + \mu_0 \sigma_e \Delta \mathbf{A} \cdot \mathbf{J}\right) d\mathbf{x} - \eta \left\|\nabla \mathbf{v}\right\|_{L^2}^2 - M \left\|\nabla\left(\omega + cf\right)\right\|_{L^2}^2 - k\left\|\nabla T\right\|_{L^2}^2 - \sigma_e \left\|\nabla \Phi\right\|_{L^2}^2 - \left\|\nabla \mathbf{A}\right\|_{L^2}^2 \tag{26}$$

where $E = \frac{\rho}{2}\left\|\mathbf{v}\right\|_{L^2}^2 + \frac{\varepsilon}{2}\left\|\nabla f\right\|_{L^2}^2 + \int_\Omega \left(\psi + \rho H f T\right) d\mathbf{x}, \psi = \frac{1}{4\varepsilon}\left(f^2 - 1\right)^2$.

E is the total free energy including kinetic energy, heat energy, the free interface energy (with an extra term representing thermocapillary effect) contributes to the mixture energy but sometimes it is the total energy when this system does not consider the extra force such as gravity and so on. Through the examples in Section 4, we will show that the total free energy (E) increases by time during the simulation where meanwhile the total energy that is the sum of total free energy and the whole work done to the system for gravity, electromagnetic force (Q in Section 3) decreases by time due to the first term in the right hand side of Eq. (26).

III. FINITE ELEMENT SCHEME, FULLY DISCRETIZED GMAW and DISCRETE ENERGY LAW

Like what we did in [15], we rewrite the continuity condition Eq. (7) with penalty formulation to enhance the stability in the computation of pressure which reformulates this problem from index-2 problem to an index-1 problem with $\nabla \cdot \mathbf{v} + \delta p = 0$ where $\delta = 10^{-6}$ is a small penalty. The solution of the weak form is approximated by a finite difference scheme in time and a conformal C^0 finite element method in space. Please see more details about the finite element space in [15]. $\Delta t > 0$ denotes the time step size and $\mathbf{v}_h^n, p_h^n, f_h^n, \omega_h^n, \mathbf{J}_h^n, \mathbf{B}_h^n, \mathbf{A}_h^n, T_h^n, \Phi_h^n$ is an approximation of $\mathbf{v}\left(t^n\right) = \mathbf{v}\left(n\Delta t\right)$, $\mathbf{v}\left(t^n\right) = \mathbf{v}\left(n\Delta t\right), p\left(t^n\right) = p\left(n\Delta t\right), \Phi\left(t^n\right) = \Phi\left(n\Delta t\right), f\left(t^n\right) = f\left(n\Delta t\right), \omega\left(t^n\right) = \omega\left(n\Delta t\right), \mathbf{J}\left(t^n\right) = \mathbf{J}\left(n\Delta t\right), \mathbf{B}\left(t^n\right) = \mathbf{B}\left(n\Delta t\right)$, $\mathbf{A}\left(t^n\right) = \mathbf{A}\left(n\Delta t\right), T\left(t^n\right) = T\left(n\Delta t\right)$. And $\mathbf{v}_h^{n+1}, p_h^{n+1}, f_h^{n+1}, \omega_h^{n+1}, \mathbf{J}_h^{n+1}, \mathbf{B}_h^{n+1}, \mathbf{A}_h^{n+1}, T_h^{n+1}, \Phi_h^{n+1}$ is the

ISSN: 2349-3224 || www.ijaetmas.com || Volume 04 - Issue 09 || September-2017 || PP. 33-42

approximation at time $t^{n+1}=(n+1)\Delta t$. The modified midpoint scheme [15] is applied in the weak form and the discretized formulation as follows

$$\int_\Omega \left(\nabla\cdot\mathbf{v}_h^{n+1/2}+\delta p_h^{n+1/2}\right)q d\mathbf{X}=0 \tag{27}$$

$$\int_\Omega\Big(\rho\mathbf{v}_{\bar{t}}^{n+1}\cdot\mathbf{u}+\rho\left(\mathbf{v}_h^{n+1/2}\cdot\nabla\right)\mathbf{v}_h^{n+1/2}\cdot\mathbf{u}+\frac{\rho}{2}\left(\left(\nabla\cdot\mathbf{v}_h^{n+1/2}\right)\mathbf{v}_h^{n+1/2}\right)\cdot\mathbf{u}-p_h^{n+1/2}\left(\nabla\cdot\mathbf{u}\right)+\eta\nabla\mathbf{v}_h^{n+1/2}:\nabla\mathbf{u}-\rho\mathbf{G}\cdot\mathbf{u}-\left(\mathbf{J}_h^{n+1/2}\times\mathbf{B}_h^{n+1/2}\right)\cdot\mathbf{u}$$

$$-\left(\omega_h^{n+1/2}+cf_h^{n+1/2}\right)\nabla f_h^{n+1/2}\cdot\mathbf{u}\Big)d\mathbf{x}=0 \tag{28}$$

$$\int_\Omega\left(f_{\bar{t}}^{n+1}\gamma+\left(\mathbf{v}_h^{n+1/2}\cdot\nabla f_h^{n+1/2}\right)\gamma+M\nabla\left(\omega_h^{n+1/2}+cf_h^{n+1/2}\right)\cdot\nabla\gamma\right)d\mathbf{x}=0 \tag{29}$$

$$\int_\Omega\left(\left(\omega_h^{n+1/2}+cf_h^{n+1/2}\right)\chi-P\left(f_h^{n+1},\,f_h^{n}\right)\chi-\varepsilon\nabla f_h^{n+1/2}\cdot\nabla\chi\right)d\mathbf{x}=0 \tag{30}$$

$$\int_\Omega\left(\rho c_p\left(T_{\bar{t}}^{n+1}+\mathbf{v}_h^{n+1/2}\cdot\nabla T_h^{n+1/2}\right)\theta+k\nabla T_h^{n+1/2}\cdot\nabla\theta+\rho H f_{\bar{t}}^{n+1}\theta-\frac{\left|\mathbf{J}_h^{n+1}\right|^2+\left|\mathbf{J}_h^{n}\right|^2}{2\sigma_e}\theta-\frac{5k_b}{2e}\mathbf{J}_h^{n+1/2}\cdot\nabla T_h^{n+1/2}\theta\right)d\mathbf{x}=0$$

(31)

$$\int_\Omega\left(\nabla\mathbf{A}_h^{n+1/2}:\nabla\boldsymbol{\alpha}+\mu_0\sigma_e\nabla\Phi_h^{n+1/2}\cdot\boldsymbol{\alpha}\right)d\mathbf{x}-\int_\Gamma\left(\mathbf{n}\cdot\nabla\mathbf{A}_h^{n+1/2}\right)\cdot\boldsymbol{\alpha}ds=0,$$

$$\int_\Omega\left(\sigma_e\nabla\Phi_h^{n+1/2}\cdot\nabla\varphi\right)d\mathbf{x}-\int_\Gamma\sigma_e\left(\mathbf{n}\cdot\nabla\Phi_h^{n+1/2}\right)\varphi ds=0, \tag{32}$$

$$\int_\Omega\left(\mathbf{J}_h^{n+1/2}+\sigma_e\nabla\Phi_h^{n+1/2}\right)\cdot\mathbf{S}\,d\mathbf{x}=0,\quad\int_\Omega\left(\mathbf{B}_h^{n+1/2}-\nabla\times\mathbf{A}_h^{n+1/2}\right)\cdot\mathbf{L}\,d\mathbf{x}=0 \tag{33}$$

where

$$\mathbf{v}_h^{n+1/2}=\frac{\mathbf{v}_h^{n+1}+\mathbf{v}_h^{n}}{2},\ p_h^{n+1/2}=\frac{p_h^{n+1}+p_h^{n}}{2},\ \mathbf{v}_{\bar{t}}^{n+1}=\frac{\mathbf{v}_h^{n+1}-\mathbf{v}_h^{n}}{\Delta t},\ \mathbf{J}_h^{n+1/2}=\frac{\mathbf{J}_h^{n+1}+\mathbf{J}_h^{n}}{2},\ \mathbf{B}_h^{n+1/2}=\frac{\mathbf{B}_h^{n+1}+\mathbf{B}_h^{n}}{2},\ T_h^{n+1/2}=\frac{T_h^{n+1}+T_h^{n}}{2},\ f_h^{n+1/2}=\frac{f_h^{n+1}+f_h^{n}}{2},$$

$$\Phi_h^{n+1/2}=\frac{\Phi_h^{n+1}+\Phi_h^{n}}{2},\ \mathbf{A}_h^{n+1/2}=\frac{\mathbf{A}_h^{n+1}+\mathbf{A}_h^{n}}{2},\ f_{\bar{t}}^{n+1}=\frac{f_h^{n+1}-f_h^{n}}{\Delta t},\ T_{\bar{t}}^{n+1}=\frac{T_h^{n+1}-T_h^{n}}{\Delta t},\ P\left(f_h^{n+1},\,f_h^{n}\right)=\frac{1}{4\varepsilon}\left(f_h^{n+1}+f_h^{n}\right)\left(\left|f_h^{n+1}\right|^2+\left|f_h^{n}\right|^2-1\right)$$

.

Be similar to the process of the derivation of the continuous energy law Eq. (26), we let $\mathbf{v}=\mathbf{u}_h^{n+1/2}, q=p_h^{n+1/2}, \chi=f_{\bar{t}}^{n+1}, \quad \gamma=\omega_h^{n+1/2}+cf_h^{n+1/2}, \theta=T_h^{n+1/2}, \varphi=\Phi_h^{n+1/2}, \boldsymbol{\alpha}=\mathbf{A}_h^{n+1/2}, \mathbf{S}=\mathbf{J}_h^{n+1/2}, T=T_h^{n+1/2}$ and then we obtain the discrete energy law

$$\frac{E^{n+1}-E^{n}+Q^{n+1}-Q^{n}}{\Delta t}=-\eta\left\|\nabla\mathbf{v}_h^{n+1/2}\right\|_{L^2}^2-M\left\|\nabla\left(\omega_h^{n+1/2}+cf_h^{n+1/2}\right)\right\|_{L^2}^2-\delta\left\|p_h^{n+1/2}\right\|_{L^2}^2-k\left\|\nabla T_h^{n+1/2}\right\|_{L^2}^2-\sigma_e\left\|\nabla\Phi_h^{n+1/2}\right\|_{L^2}^2-\left\|\nabla\mathbf{A}_h^{n+1/2}\right\|_{L^2}^2 \tag{34}$$

$$E^i=\frac{\rho}{2}\left\|\mathbf{v}_h^i\right\|_{L^2}^2+\frac{\varepsilon}{2}\left\|\nabla f_h^i\right\|_{L^2}^2+\int_\Omega\left(\frac{1}{4\varepsilon}\left(\left|f_h^i\right|^2-1\right)^2+\rho H f_h^i T_h^i\right)d\mathbf{x},$$

ISSN: 2349-3224 || www.ijaetmas.com || Volume 04 - Issue 09 || September-2017 || PP. 33-42

(35)

$$Q^i = -\sum_{k=0}^{i-1} \int_\Omega \Delta t \left(\rho \mathbf{G} \cdot \mathbf{v}_h^{k+1/2} + \left(\mathbf{J}_h^{k+1/2} \times \mathbf{B}_h^{k+1/2} \right) \cdot \mathbf{v}_h^{k+1/2} + \mu_0 \sigma_e \Delta \mathbf{A}_h^{k+1/2} \cdot \mathbf{J}_h^{k+1/2} \right) d\mathbf{x}$$

(36)

Here E is the total free energy at each time step and Q represents the work done by gravity and electromagnetic force accumulation of time. And we can see that this discrete energy law Eq. (34) is almost the same as the continuous energy law Eq. (26). We apply a fixed point method in the linearization process results in the linear system by a carefully designed fixed point method do not depend on the time and we just do the LU factorization once at the initial time step.

IV. METAL TRANSFER and DISCUSSION

In this section, we simulate the process of metal transfer in GMAW to show the accuracy of the model, energy law preserving method and the scheme. Constant current (200A) is set as the welding current and the electrode is stainless steel with the diameter 1.2mm. The initial arc length is 3mm and the shielding gas is pure argon. The computations are carried out with the help of FreeFem++ platform and shown with Tecplot. $\mathbf{v}, f, \omega, \mathbf{J}, \mathbf{B}, \mathbf{A}, T, \Phi$ are computed under the P_2 (piecewise polynomial of degree two) finite element space and the P_1 finite element space for p. We use Eq. (27)-(33) to compute this example with a relative coarse grid 32×32 compared with the finer grid in [4] and the evolution of the interface of the drop is shown in Fig. 2. As the interface having thickness, we choose the $f = 0$ as the position of the interface. The numerical simulation agreed well with the theory of the metal transfer in GMAW as we can see the metal melting, drop coming out, necking effect and the breaking up of the drop. In Fig. 3, we show the evolution of total free energy, total energy and the error in the energy law by time. As the error in the energy law falls down to 10^{-8}, the accuracy of the continuous energy law and the discrete energy law is validated.

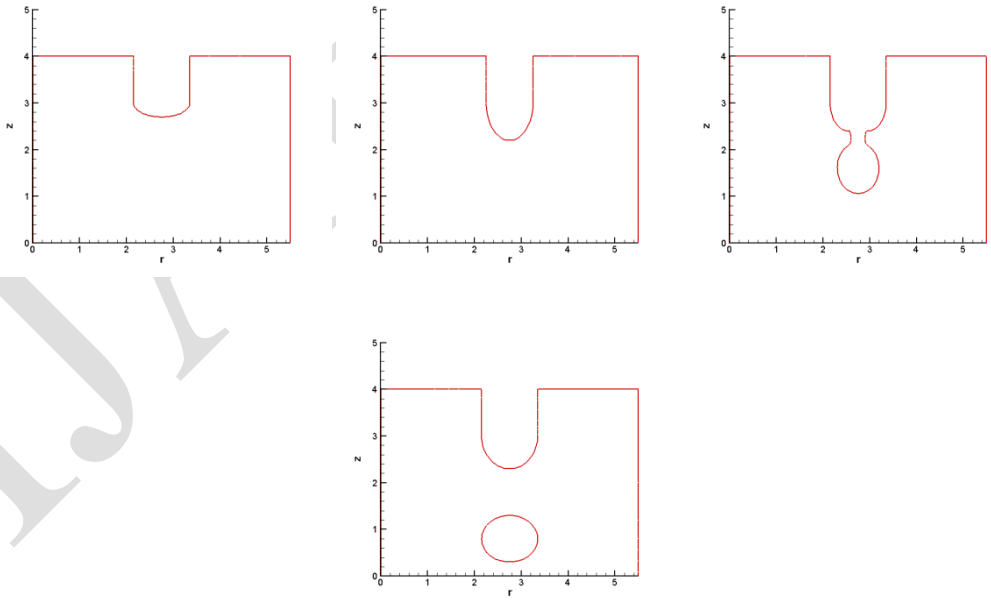

Fig. 2 The metal transfer and the interface with constant current at $t = 92.332, 93.709, 96.448, 99.563$ms .

We also compared the numerical solution like the breaking up time and the diameter of the drop (the average value of horizontal and vertical diameter from 3000 drops) with the data of high-speed photography (Fig. 4). The result is shown in Table 1. The comparison shows that the result of numerical simulations agreed well with

ISSN: 2349-3224 || www.ijaetmas.com || Volume 04 - Issue 09 || September-2017 || PP. 33-42

experiment data and the error maybe comes from the lack of applied force on the drop like plasma force and also some unpredictable factor such as the influence of short circuiting transfer on the later process and the fume.

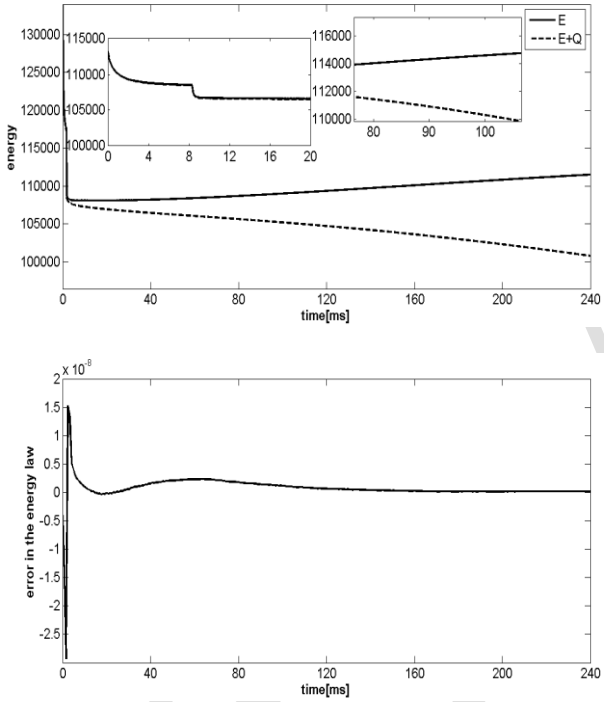

Fig. 3 Left: The evolution of total free energy and total energy; Right: The error in the discrete energy law.

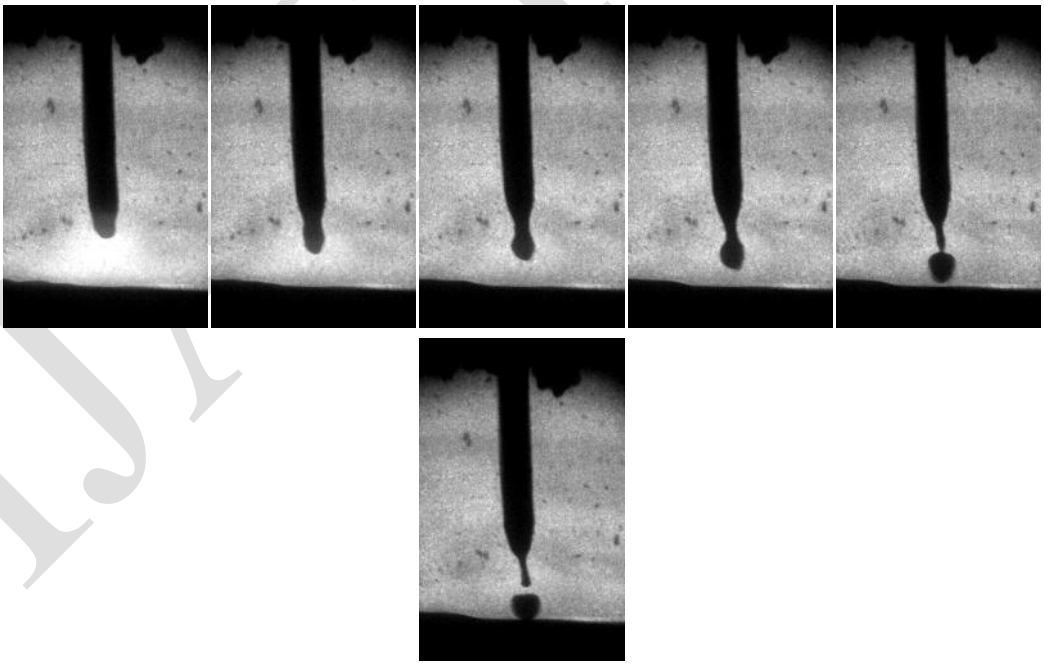

Fig. 4 Metal transfer captured by the high-speed photography.

ISSN: 2349-3224 || www.ijaetmas.com || Volume 04 - Issue 09 || September-2017 || PP. 33-42

TABLE I

COMPARISON BETWEEN NUMERICAL SIMULATIONS and HIGH-SPEED PHOTOGRAPHY.

	Horizontal Diameter	Vertical Diameter	Breaking Up Time
Numerical Simulations	1.217mm	1.013mm	98.105ms
High-speed Photography	1.152mm	1.002mm	96.773ms

V. CONCLUSIONS

In this paper, we derive an energy law for GMAW with phase field model and use a modified midpoint scheme to get the continuous and discrete energy law. We use this energy law preserving finite element method to compute the GMAW system with constant current based on a relative coarse grid like 32×32 and simulate the metal transfer process which agrees well with the theory of metal transfer. We also compare the numerical solutions with the data of high-speed photography like the diameter of detachment drop and the breaking up time. The comparison shows the accuracy of the model, the energy law preserving method, the energy law and the computation in this paper would have a higher computing efficiency as we use the relative coarser grid than the work in the reference.

ACKNOWLEDGEMENT

Yongyue Jiang is partially supported by Beijing Postdoctoral Research Foundation.

REFERENCE

[1] J. Mckelliet and J. Szekely, "Heat transfer and fluid flow in the welding arc," Metallurgical Transactions A, vol. 17, 1986, pp. 1139-1148.

[2] J. Haidar and J.J. Lowke, "Predictions of metal droplet formation in arc welding," Journal of Physics D: Applied Physics, vol. 29, 1999, pp. 1233-1244.

[3] M. Chen, C. Wu and R. Lian, "Numerical analysis of dynamic process of metal transfer in GMAW," Acta Metallrugica Sinica, vol. 40, 2004, pp. 1227-1232.

[4] J. Hu and H. Tsai, "Heat and mass transfer in gas metal arc welding. Part I the arc," International Journal of Heat and Mass Transfer, vol. 50, 2007, pp. 833-846.

[5] A.B. Murphy, "A self-consistent three-dimensional model of the arc, electrode and weld pool in gas metal arc welding," Journal of Physics D: Applied Physics, vol. 44, 2011, pp. 252-260.

[6] J. Haidar, "An analysis of heat transfer and fume production in gas metal arc welding. III," Journal of Applied Physics, vol. 85, 1998, pp. 3448-3459.

[7] Z. Guo , P. Lin and Y. Wang, "Continuous finite element schemes for a phase field model in two-layer fluid Benard Marangoni convection computations, " Computer Physics Communications, vol. 185, 2014, pp. 63-78.

[8] R. Borcia, D. Merkt and M. Bestehorn, "A phase-field description of surface-tension-driven instability," International Journal of Bifurcation & Chaos, vol. 14, 2004, pp. 4105-4116.

[9] Z. Guo and P. Lin, "A thermodynamically consistent phase-field model for two-phase flows with thermocapillary effects," Journal of Fluid Mechanics, vol. 766, 2015, pp. 226-271.

[10] Z. Guo, P. Lin and J.S. Lowengrub, "A numerical method for the quasi-incompressible Cahn-Hilliard-Navier-Stokes equations for variable density flows with a discrete energy law," Journal of Computational Physics, vol. 276, 2014, pp. 486-507.

ISSN: 2349-3224 || www.ijaetmas.com || Volume 04 - Issue 09 || September-2017 || PP. 33-42

[11] Z. Guo, P. Lin and Y. Wang, "Continuous finite element schemes for a phase field model in two-layer fluid Benark-Marangoni convection computations," Computer Physics Communications, vol. 185, 2014, pp. 63-78.

[12] Z. Guo, P. Lin, S. Wise and J. Lowengrub, "Mass conservative and energy stable finite difference methods for the quasi-incompressible Navier-Stokes-Cahn-Hilliard system: primitive variable and projection type schemes," Computer Methods in Applied Mechanics and Engineering, in press, 2017.

[13] F. Chen and J. Shen, "Efficient energy stable schemes with spectral discretization in space for anisotropic Cahn-Hilliard systems," Communications in Computational Physics, vol. 13, 2013, pp. 1189-1208.

[14] G. Beckett, J. Mackenzie and M. Robertson, "An r-adaptive finite element method for the solution of the weo-dimensional phase-field equations," Communications in Computational Physics, vol. 1, 2006, pp. 805-826.

[15] Y. Jiang, P. Lin, Z. Guo and S. Dong, "Numerical simulation for moving contact line with continuous finite element schemes," Communications in Computational Physics, vol. 18, 2015, pp. 180-202.

[16] J. Kim, K. Kang and J. Lowengrub, "Conservative multi-grid methods for Cahn-Hilliard fluids," Journal of Computational Physics, vol. 193, 2004, pp. 511-543.

[17] H. Yu and X. Yang, "Numerical approximations for a phase field moving contact line model with variable densities and viscosities," Journal of Computational Physics, vol. 334, 2017, pp. 665-686.

[18] P. Lin, C. Liu and H. Zhang, "An energy law preserving C^0 finite element scheme for simulating the kinematic effects in liquid crystal flow dynamics," Journal of Computational Physics, vol. 227, 2007, pp. 1411-1427.

[19] J. Hua, P. Lin, C. Liu and Q. Wang, "Energy law preserving C^0 finite element schemes for phase field models in two-phase flow computations," Journal of Computational Physics, vol. 230, 2011, pp. 7115-7131.